JCTC Journal of Chemical Theory and Computation

Article

pubs.acs.org/JCTC

Critical Comparison of Biomembrane Force Fields: Protein−Lipid Interactions at the Membrane Interface

Angelica Sandoval-Perez, Kristyna Pluhackova, and Rainer A. Böckmann*

Computational Biology, Department of Biology, Friedrich-Alexander University of Erlangen-Nürnberg, Staudtstrassre 5, 91058 Erlangen, Germany

Supporting Information

ABSTRACT: Molecular dynamics (MD) simulations offer the possibility to study biological processes at high spatial and temporal resolution often not reachable by experiments. Corresponding biomolecular force field parameters have been developed for a wide variety of molecules ranging from inorganic ligands and small organic molecules over proteins and lipids to nucleic acids. Force fields have typically been parametrized and validated on thermodynamic observables and structural characteristics of individual compounds, e.g. of soluble proteins or lipid bilayers. Less strictly, due to the added complexity and missing experimental data to compare to, force fields have hardly been tested on the properties of mixed systems, e.g. on protein−lipid systems. Their selection and combination for mixed systems is further complicated by the partially differing parametrization strategies. Additionally, the presence of other compounds in the system may shift the subtle balance of force field parameters. Here, we assessed the protein−lipid interactions as described in the four atomistic force fields GROMOS54a7, CHARMM36 and the two force field combinations Amber14sb/Slipids and Amber14sb/Lipid14. Four observables were compared, focusing on the membrane-water interface: the conservation of the secondary structure of transmembrane proteins, the positioning of transmembrane peptides relative to the lipid bilayer, the insertion depth of side chains of unfolded peptides absorbed at the membrane interface, and the ability to reproduce experimental insertion energies of Wimley-White peptides at the membrane interface. Significant differences between the force fields were observed that affect e.g. membrane insertion depths and tilting of transmembrane peptides.

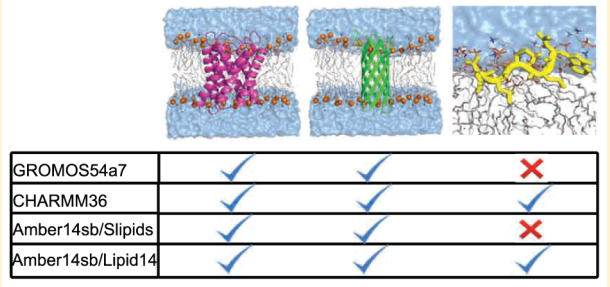

1. INTRODUCTION

The increase of computational resources in terms of hardware and algorithms as well as the boost in the development and further refinement of force field parameters enable us nowadays to reliably study *in silico* protein dynamics at the atomistic scale in a nativelike environment. Transmembrane proteins constitute 20 to 30% of all encoded proteins.[1] Therefore, a proper parametrization of protein−lipid interactions is of high interest. Apart from determining protein localization, lipids frequently even modulate protein activity,[2] e.g. by influencing the protein insertion depth.[3] One example is the GPCR β_2 adrenergic receptor. Its activation is favored by negatively charged lipids. The receptor may also be activated by detergents in the absence of a membrane.[4,5] Similarly, the functioning of the chemokine receptor CXCR4 is coupled to membrane cholesterol.[6] Molecular dynamics (MD) simulations using a sequential multiscaling approach suggested that the steroid drives the formation of an activation-competent dimerization interface.[7]

Attempts to understand the role of lipids in the activation of the β_2-adrenergic receptor by simulations revealed a huge influence of the results on the particular force field: the number of lipid binding events to a specific binding pocket within the receptor was reported to be reduced or enlarged by up to 1 order of magnitude for different force fields.[8] However, it is difficult to assess different protein−lipid force fields, based on results obtained for specific observables of selected proteins.

Biomolecular force fields are continuously developed since the mid 1970s.[9,10] Initially, the development of parameters mainly focused on the reproduction of *ab initio* data for small molecules and protein structural data.[11−13] The second generation of force fields, developed from the beginning of the 1990s, aimed to reproduce besides structure also thermodynamic properties like densities and hydration free energies, thereby enabling the study of condensed states. Simulations of systems in their condensed state require a fine balance between solvent−solute, solute−solute, and solvent−solvent interactions.[14,15] Although increased attention was attributed to protein−lipid−water interactions during the last years, the force field refinement is limited by the lack of experimental data for general observables such as e.g. the insertion depths of different transmembrane (TM) peptides. Therefore, the calibration and the validation of force fields focused mainly on the reproduction of properties of either water solvated proteins or of pure membrane characteristics. For proteins, force fields are typically evaluated in terms of

Received: January 2, 2017
Published: April 7, 2017

DOI: 10.1021/acs.jctc.7b00001
J. Chem. Theory Comput. 2017, 13, 2310−2321

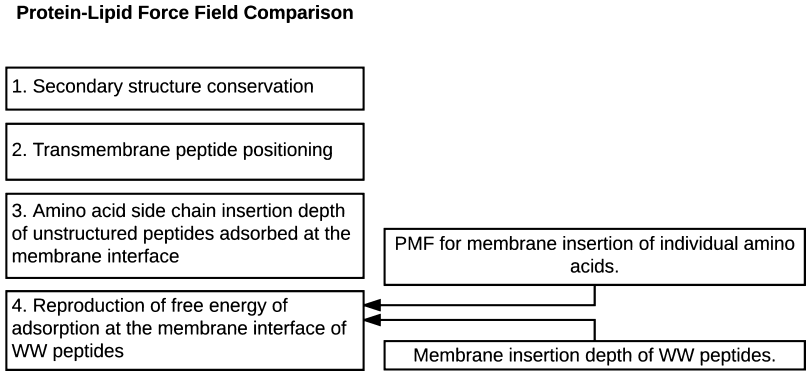

Figure 1. Analysis performed in the assessment of different protein−lipid force fields.

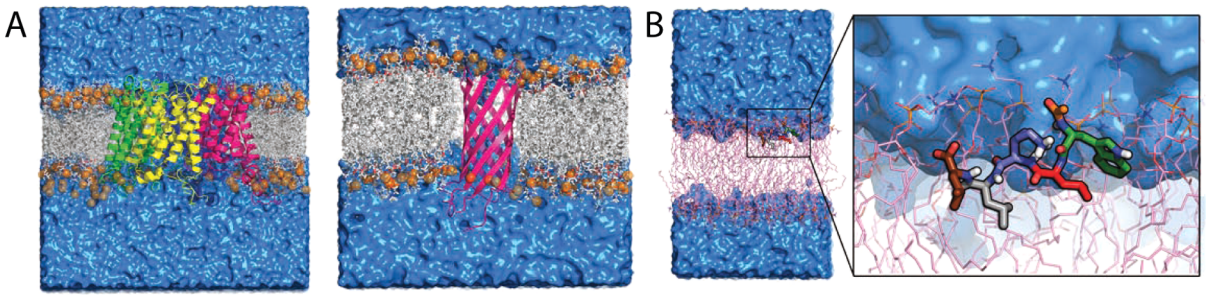

Figure 2. (A) Transmembrane protein systems used to analyze the conservation of a secondary structure in different force fields. AQP0 on the left and OmpX on the right (shown as chain-colored cartoons) were inserted into a model POPC bilayer (shown as gray sticks with phosphate atoms highlighted as orange spheres) and solvated by water (shown as marine surface) at 150 mM NaCl (omitted for clarity). (B) Sample Wimley-White peptide-membrane system. The membrane is shown as element-colored sticks (carbon in pink, nitrogen in blue, oxygen in red, and phosphorus in orange). The amino acid coloring of the peptide is as follows: acetyl in orange, tryptophan (residue 1) in green, leucine (residue 2) in red, lysine (residue 3) in purple, leucine (residue 4) in gray, and leucine with negatively charged C-terminus (residue 5) in brown.

secondary structure reproducibility.[16−21] Recently, also structural observables of intrinsically disordered peptides and proteins were assessed.[22,23] For membranes, the area per lipid, volume per lipid, surface tension, electron density, order parameters, X-ray and neutron scattering form factors, and lipid diffusion are typically compared to experiments.[24−30] Current attempts to validate all-atom force fields that include protein−lipid interactions are restricted to the structural characteristics of membrane-embedded proteins or peptides.[31] Differently, the evaluation of the quality of the Martini coarse-grained force field[32] and later on the reparametrization of the protein parameters (version 2.2[33]) was validated by the partition free energies of model Wimley-White (WW) peptides[34] at solvent−water or at the membrane-water interface. In contrast, the estimation of insertion free energies of full-length WW peptides is currently hardly feasible in atomistic MD simulations.[35] All-atom approaches therefore used simplified systems consisting of single amino acid side chain analogs only to assess protein or peptide membrane insertion free energies.[36,37] Possible artifacts due to the exclusion of backbone energy contributions as well as the neglect neighboring amino acids are difficult to quantify.

Here, we compared different protein−lipid force field combinations: (1) in their ability to conserve the secondary structure of selected transmembrane proteins, (2) in the positioning of transmembrane peptides in the lipid bilayer and their influence on the lipid surrounding, (3) for differences in the insertion depth of the side chains of unstructured peptides absorbed at the bilayer interface, and (4) their ability to reproduce the insertion free energies of Wimley-White (WW) peptides. The peptide insertion free energies were approximated by the sum of the energies of individual amino acids, weighted by their membrane depth distribution in WW peptides. The potential of the mean force (PMF) for the membrane insertion of individual capped amino acids was analyzed at atomistic resolution, taking for the first time the backbone contributions into account. Four force fields commonly used to simulate protein−membrane systems were compared, namely the united-atom GROMOS54a7,[16] the all-atom CHARMM36,[38] and the two all-atom combinations Amber14sb/Slipids[39,40] and Amber14sb/Lipid14.[26,39]

2. MATERIALS AND METHODS

The analysis performed in the assessment of different force fields in the study of protein−lipid interactions is summarized in Figure 1. This section summarizes the preparation, simulation, and analysis of the different simulation systems used for these tests. In detail, transmembrane proteins, helical transmembrane peptides, membrane-absorbed short peptides, and single capped amino acids were studied.

2.1. Transmembrane Protein Simulations. The ability of the studied force fields to preserve the secondary structure of transmembrane (TM) proteins was analyzed based on MD simulations of a β-barrel membrane protein (OmpX, pdb entry 2M06[41]) and a protein with excess of α-helical structure (aquaporine, AQP0, pdb entry 2B6P[42]) embedded in a lipid bilayer (see Figure 2 A). The TM protein simulations were prepared using our recently established procedure.[43] In brief, the proteins were converted to the coarse-grained (CG) Martini representation (Martini2.2 force field[44]) using *martinize*.[44] Next, a 1-phosphatidyl-2-oleoyl-*sn*-glycero-3-phos-

DOI: 10.1021/acs.jctc.7b00001
J. Chem. Theory Comput. 2017, 13, 2310−2321

Table 1. Simulation Conditions for Individual Force Fields[e]

parameters	GROMOS54a7	CHARMM36	Amber14sb/Lipid14	Amber14sb/Slipids
time step [fs]	2	2	2	2
$R_{Coulomb}$ [nm]	1.4	1.2	1.0	1.5
Coulomb method	GRF[57](ϵ_{RF} = 61)	PME[58]	PME[58]	PME[58]
R_{vdW} [nm]	1.4	0.8−1.2	1.0	1.5
vdW method	Verlet cutoff[60]	Verlet cutoff[a60]	Verlet cutoff	Verlet cutoff[a60]
vdW modifier		switch		switch
dispersion correction	no	no	EnerPress[61]	EnerPress[61]
COM removal[b][steps]	100	100	100	100
neighbor list search [steps]	10	10	10	10
barostat	Berendsen[46]	PR[59]	Berendsen[46]	PR[59]
τ_p [ps]	0.5	5	1	10
thermostat[d]	Berendsen[46]	Nosé-Hoover[62,63]	Nosé-Hoover[62,63]	Nosé-Hoover[62,63]
τ_T [ps]	0.1	0.5	0.5	0.5
constraints	h-bonds	h-bonds	h-bonds	all bonds
water model	SPC[64]	TIP3P[c65]	TIP3P[66]	TIP3P[66]
ion model	GROMOS54a7	CHARMM36	Amber99sb	Amber99sb

[a]The Verlet cutoff scheme[60] in combination with a switch vdW modifier is equal to the old switch scheme for van der Waals interactions. [b]The COM (center of mass) motion was removed linearly for the whole system. [c]The CHARMM TIP3P water model with Lennard-Jones interaction sites on hydrogens. [d]For membrane proteins the v-rescale thermostat was used due to better lipid entropy conservation (data not shown). [e]GRF,[57] generalized reaction field; PME,[58] particle-mesh Ewald; PR,[59] Parrinello−Rahman thermostat; vdW, van der Waals interactions.

phocholine (POPC) lipid bilayer was built, and coarse-grained water molecules and ions (corresponding to 150 mM NaCl concentration in the atomistic representation) were added using the program *insane*.[45] The systems were energy minimized using 500 steps of a steepest descent minimization. A set of position restraint simulations (2,000 steps each) with increasing simulation time steps, namely 2, 10, and 20 fs, was performed followed by 350 ns equilibration simulations. The simulations were performed in an NpT ensemble, applying a semiisotropic pressure coupling to 1 bar using the Berendsen barostat[46] with a coupling time constant of 3 ps. The temperature was kept constant at 310 K separately for the protein, the lipid bilayer, and water with ions using the Berendsen thermostat[46] with a coupling time constant of 1 ps. However, note that the Berendsen thermostat and barostat do not strictly provide a correct thermodynamic ensemble. The center of mass of the system was removed in every step separately for the membrane-protein system and the water phase. The electrostatic interactions were shifted between 0 and 1.2 nm and the van der Waals interactions between 0.9 and 1.2 nm to zero. The relative dielectric constant was set to 15, and the nonbonded interaction list was updated every 10 integration steps.

After equilibration in the CG representation, the systems were converted to atomistic resolutions applying the *backward* method.[47] In the backmapped structures the CG protein was replaced by its crystal structure, and the system was twice minimized. During the first minimization of 200 steps the protein crystal structure was kept frozen. In the second minimization (200 steps of steepest descent minimization) all atoms were allowed to move freely. Two ns position restraint simulations were followed by production simulations (200 ns in the case of OmpX and 100 ns in the case of the aquaporin tetramer). The simulation parameters for all studied force fields, namely GROMOS54a7,[16] CHARMM36,[38] Amber14sb/Slipids,[39,40] and Amber14sb/Lipid14,[26,39] are summarized in Table 1. For GROMOS54a7 and CHARMM36 standard ion parameters included in the force field were used. For simulations with the Amber14sb protein force field, the ion parameters (mostly based on the ion parameters developed by Åqvist[48]) from the Amber99sb force field were used instead of the Joung and Cheatham ion parameters[49] that are included in the GROMACS' version of Amber14sb. The reason for this choice is the original parametrization and the validation of the Lipid14 and Slipids lipid parameters with the Amber99sb ion parameters.[50,51] The Joung and Cheatham parameters led to excessive overbinding of ions to the lipid membrane. Further information on the influence of the ion parameters on protein−membrane simulations is included in the Supporting Information.

2.2. Transmembrane Peptide Simulations. The effect of different force fields on the relative positioning of transmembrane peptides was exemplarily evaluated for a model WALP23 peptide spanning a DOPC bilayer and a polyvaline mutant of the transmembrane domain of synaptobrevin (sybII) embedded in a POPC bilayer. The latter peptide was shown to have a large impact on the membrane structure.[52] The WALP23 (1-GWWLALALALALALALALALWWA-23) and the synaptobrevin transmembrane segment (88-YWWKNL-KMMVVVVVVVVVVVVVVVYFST-116) were modeled in α-helical conformation using PyMOL.[53] The peptides were transformed to a coarse-grained representation (Martini 2.2 force field) with *martinize*[44] and surrounded by a DOPC (WALP23) or a POPC (sybII polyV mutant) bilayer, hydrated with water and 150 mM NaCL using *insane*.[45] After equilibration of the CG representation, the systems were converted to atomistic resolution using *backward*[47] (for CHARMM36 and GROMOS54a7 force fields). A snapshot of the simulated system using CHARMM36 was converted to representations compatible with Amber14sb/Slipids and Amber14sb/Lipid14. The simulation workflow was identical to the one used for the TM protein simulations. The simulation parameters used for the force fields are listed in Table 1. The production simulations lasted for 500 ns for each system. Synaptobrevin was simulated at 310 K and WALP23 at 313 K.

2.3. Insertion Depth of Oligopeptides at the Membrane Interface. A CG representation of a Wimley-White (WW) peptide, structure Ace-W_1-L_2-X_3-L_4-L_5-COO^-(where X_3

DOI: 10.1021/acs.jctc.7b00001
J. Chem. Theory Comput. 2017, 13, 2310−2321

is the amino acid of interest), absorbed on a bilayer of 128 POPC lipids and hydrated with 80 water molecules per lipid, was obtained from Gurpreet Singh (personal communication).[32] Additionally, three selected dipeptides, Ace-W-L-NH_2, Ace-S-L-NH_2, and Ace-L-L-COO^-, adsorbed on a bilayer of 200 POPC lipids, hydrated with 85 water molecules per lipid were prepared. The CG structures of WW peptides were converted to atomistic resolution for the different studied atomistic force fields, while the selected dipeptides were converted exclusively to atomistic descriptions within the CHARMM36 force field. The conversion succeeded by the tool *backward*.[47] The atomistic Wimley-White peptides (see Figure 2 B) were capped with an acetyl group on their N-terminus and uncapped at the C-terminus. Membrane insertion depth distributions were obtained from 500 ns equilibration MD simulations at 310 K. The progression of the insertion depths for the individual side chains was monitored as a function of time (Supporting Information). Figure 3 D exemplary shows the distributions for the WW peptide Ace-W_1-L_2-A_3-L_4-L_5-COO^- within the Amber14sb/Slipids force fields.

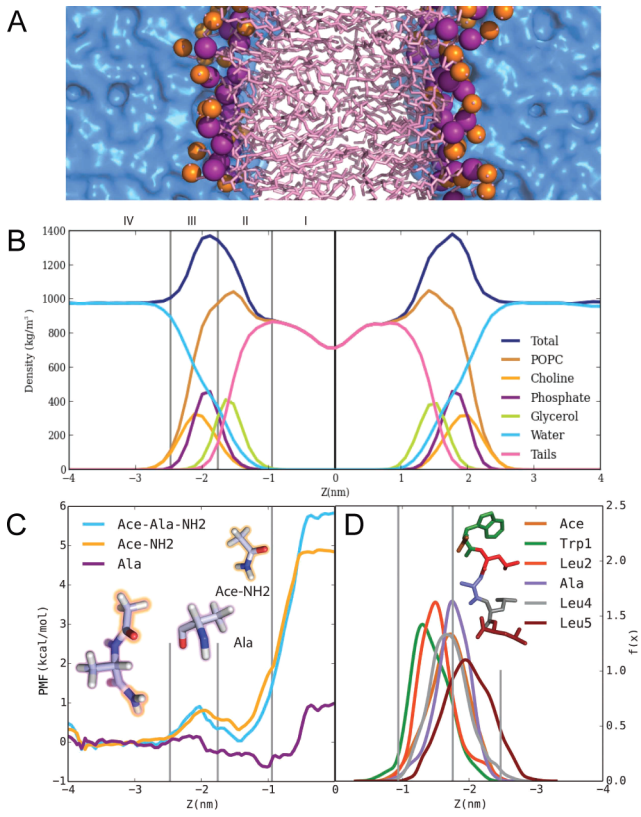

Figure 3. (A) Snapshot of the studied POPC membrane. (B) Density profile of the system used to divide the simulation box into regions I–IV. (C) Energy profiles of an acetyl amide (Ace-NH2) and of capped and uncapped alanine. (D) The insertion depth distributions of the different components of a sample WW peptide within the Amber14sb/Slipids force fields.

2.4. Energy Profiles of Individual Amino Acids. In order to calculate the potential of the mean force (PMF) of representative residues along the lipid bilayer normal, the amino acids Ala, Leu, Phe, Trp, Ser, Glu, Asp, and Lys capped with the acetyl group (N-terminus) and the amino group (C-terminus) (Figure 4 A) were positioned in the solvent phase at a distance of 5 nm from the center of mass (COM) of a POPC

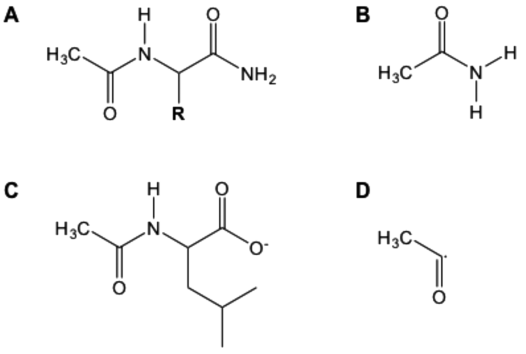

Figure 4. Chemical structures of (A) amino acids capped by acetyl and amino groups (R corresponds to the side chain of the studied residue), (B) acetyl amide, (C) leucine capped on its N-terminus with the acetyl group and carrying a negatively charged C-terminus, and (D) the acetyl radical.

bilayer (72 lipids hydrated with approximately 85 water molecules per lipid). Additionally, membrane systems containing acetyl amide, acetyl radical, and leucine capped at its N-terminus by an acetyl group and carrying a negatively charged C-terminus (Leu-COO^-) at the predefined membrane distance of 5 nm were prepared. Structures of these molecules are shown in Figure 4 B, D, and C, respectively.

The simulation systems were prepared as follows: First, CG representations of all capped amino acids were generated using *martinize*.[33] Subsequently, the lipid bilayer and water were added using *insane*.[43] Each system was energy minimized using the steepest descent algorithm for 10,000 steps and equilibrated for 10 ns applying position restraints on the backbone bead of the studied amino acid. The equilibrated CG systems were converted to an atomistic description (Amber14sb/Slipids force fields[31,39]) using the tool *backward*[47] and equilibrated with protein position restraints for 100 ps.

PMFs of the capped amino acids of the membrane normal (water phase to bilayer center) were calculated using umbrella sampling.[54,55] Starting structures for umbrella sampling simulations were generated by pulling the center of mass (COM) of each capped amino acid from water into the bilayer at a pulling rate of 0.001 nm/ps with a force constant of 1000 kJ mol^{-1} nm^{-2} for 10 ns. All pulling simulations were performed using the Amber14sb/Slipids force fields combination and the GROMACS 5.0.4 package.[56] Other simulation conditions can be found in Table 1.

Umbrella sampling was performed in the range of 0 to 4 nm of separation along the membrane normal (z) between the COM of the capped residue and the bilayers COM. The simulation system was divided into four regions based on the component density along the membrane normal, similar to Marrink et al.,[67] see Figure 3 B. Umbrella sampling starting structures were selected from the pulling simulations at spacing of ≤0.1 nm, resulting in 44 to 100 umbrellas for each amino acid. Subsequently, the snapshots were converted to representations within the three other studied force fields here, namely GROMOS54a7,[16] Amber14sb/Lipid14,[26,39] and CHARMM36.[68] The samples were equilibrated applying position restraints on the capped amino acid for 1 ns. Afterward, umbrella sampling production run simulations were performed and monitored every 1 ns until the energy at the membrane interface region varied less than 0.2 kcal/mol over the last 5 ns of the respective umbrella simulation (see Supporting Information Figures S6–S9). The production

DOI: 10.1021/acs.jctc.7b00001
J. Chem. Theory Comput. 2017, 13, 2310–2321

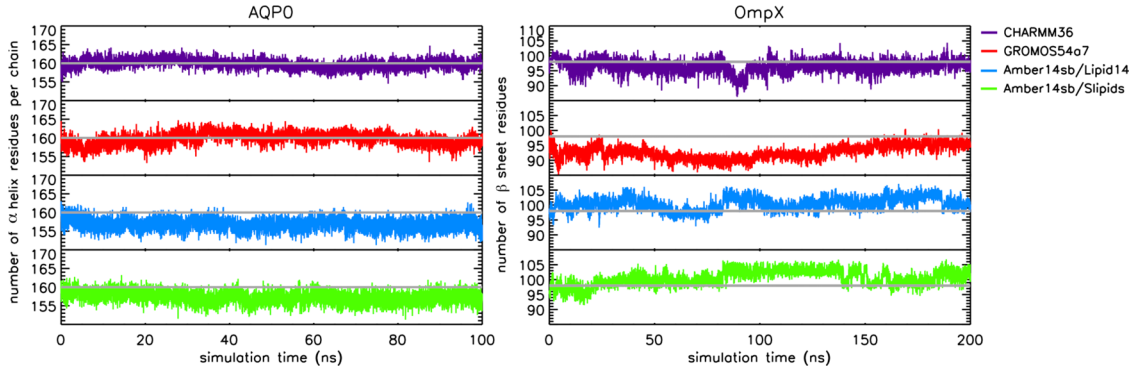

Figure 5. Conservation of a secondary structure over simulation time for the different studied force fields as determined by the program DSSP.[70] Only the main secondary structure types (α-helix in the case of AQP0 and β-sheet in the case of OmpX) are shown. The secondary structure content of the respective crystal structures is shown as gray lines. In the case of AQP0 averages over all 4 chains (identical secondary structure content in the beginning of the simulation) are shown.

simulations ranged between 20 and 40 ns for Amber14sb/Slipids, Amber14sb/Lipid14, and CHARMM36 force fields and 40 and 70 ns for GROMOS54a7 due to the reduced lipid diffusion in this force field.[28] Energy profiles were calculated using the weighted histogram analysis method (WHAM[69]). The uncertainty was calculated with 200 bootstraps, applying the Bayesian bootstrap method.[69] The energy profiles with their respective standard deviations and the histograms for each studied capped amino acid are shown in the Supporting Information.

The energy profiles for the uncapped amino acids were approximated by subtracting the profile for acetyl amide from the given capped amino acid. Figure 3 C shows the described procedure for alanine simulated in the Amber14sb/Slipids force field combination. The energy of the terminal Leu-$COO^-$was calculated by subtracting the energy profile of the acetyl radical from the profile of leucine capped on its N-terminus by the acetyl group.

2.5. Energy Profiles of Dipeptides. The potential of the mean force was further calculated for three dipeptides: Ace-W-L-NH_2, Ace-S-L-NH_2, and Ace-L-L-COO^-.

The peptides were prepared according to the protocol described in Section 2.4 for the calculation of the PMF for individual amino acids. Each dipeptide was located in water at a distance of ≈5 nm from the center of mass of a POPC bilayer consisting of 200 lipids and hydrated by approximately 85 water molecules per lipid. The pulling simulation of each dipeptide from water to the middle of the bilayer was performed using the atomistic force field CHARMM36. Each peptide was pulled into the membrane at a rate of 0.001 nm/ps with a force constant of 1,000 kJ $mol^{-1}nm^{-2}$ for 10 ns. Snapshots of the pulling process were selected at a spacing of 0.1 nm along the membrane normal. These snapshots were used as starting structures for the umbrella sampling simulations. Following an equilibration of 1 ns with position restraints on both the membrane and peptide center of masses, umbrella sampling production runs were performed until convergence of the PMF was achieved. The convergence was measured as the change in the depth of the local minima between $z = -2$ nm and $z = -1$ nm ($z = 0$ corresponds to the membrane center). The criterium for convergence was a variation <0.2 kcal/mol over the last 5 ns of the simulations (see the Supporting Information). Under this condition, the individual umbrella production runs lasted 50 ns for the dipeptides Ace-S-L-NH2 and Ace-L-L-COO- and 70 ns for Ace-W-L-NH2.

2.6. Free Energies of Absorption of Oligopeptides. The total absorption energy (E_{abs}) (see eq 1) of an oligopeptide to the membrane interface was approximated by the sum of the energy contributions for each residue (x) (i.e., the insertion energy of a WW peptide includes the contributions of acetyl radical, uncapped amino acids W, L, X, L, and L-COO^-).

These individual energy contributions were calculated by weighting the PMF of the residue ($E_x(z)$) with its normalized insertion depth distribution ($P_x(z)$) obtained from the simulation of the full peptide. The individual PMF curves were obtained from umbrella sampling simulations along the membrane normal for distances z between 0 and −4 nm from the membrane center.

$$E_{abs} = \sum_{x \epsilon X} \int_0^4 E_x(z) P_x(z) dz \quad (1)$$

3. RESULTS

3.1. Conservation of Secondary Structure. The conservation of protein secondary structure in molecular dynamics simulations is one of the most frequently applied and accepted validation methods to assess the quality of biomolecular force fields.[16−20] Figure 5 shows the α-helical and β-sheet content over the simulation time for the TM proteins AQP0 and OmpX, respectively. All investigated force fields largely conserved both the α-helical and β-sheet content during the simulation time. The variations with respect to the crystal structure (gray line) are small in most cases, and only slight differences among the force fields were observed. Namely, the α-helical content of AQP0 described by the Amber14sb force field decreased by about 3 residues per chain as compared to the crystal structure. This decrease results from a partial refolding into a 3^{10} helix (see the Supporting Information). The β-sheet content of OmpX is well conserved for all studied force fields, only GROMOS54a7 temporarily showed a reduced β-sheet content (up to 8 residues). However, the crystal β-sheet content was largely recovered during the final 50 ns of the simulation. All studied force field combinations appear well suitable in the study of both membrane embedded β-barrel and α-helical transmembrane proteins using MD simulations.

3.2. Transmembrane Peptide Positioning. Single helical peptides are more sensitive to subtle differences in protein−lipid interactions as compared to large compact transmembrane proteins. Two test systems for protein−lipid interactions at the

DOI: 10.1021/acs.jctc.7b00001
J. Chem. Theory Comput. 2017, 13, 2310−2321

Table 2. Tilt Angle of the WALP23 Peptide and a Synaptobrevin TM Mutant Peptide, Membrane Thickness of Pure POPC Membrane (PM), and Membrane Thickness in the Vicinity of the Respective Peptide within a 1 nm Distance of the Peptide (LM)[b]

	WALP23	sybII polyV mutant		
force field	tilt angle (deg)	tilt angle (deg)	PM (nm)	LM (nm)
CHARMM36	14.5 ± 3.6	26.8 ± 3.7	3.90 ± 0.02	3.90 ± 0.06
GROMOS54a7	19.8 ± 4.0	18.9 ± 3.2	3.94 ± 0.02	4.02 ± 0.04
Amber14sb/Lipid14	19.5 ± 4.5	30.2 ± 4.7	3.78 ± 0.01	3.80 ± 0.09
Amber14sb/Slipids	18.4 ± 4.7	28.6 ± 9.4	3.75 ± 0.01	3.67 ± 0.14
experiment	21 ± 3[71]		3.88[72a]	

[a]Obtained by linear extrapolation (R-squared value of 0.97) of experimental data.[72] [b]Standard deviations were determined on 50 ns intervals of the peptide and on 20 ns intervals of the pure membrane simulations.

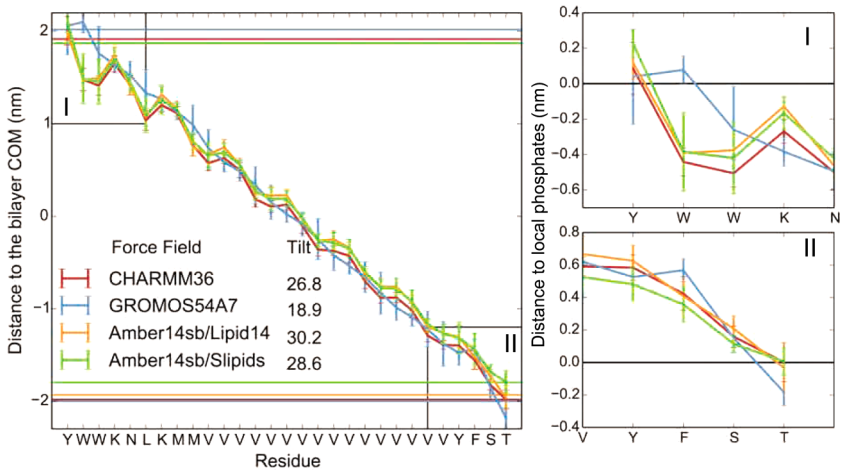

Figure 6. Distance between the POPC bilayer core, defined by the center of mass (COM) in a normal direction, and the COM of each amino acid of the transmembrane domain of a polyvaline mutant of sybII, calculated from time frames of 50 ns between 50 and 500 ns of simulation. The standard deviations are shown as error bars. The lines represent the z-positions of the COM of lipid phosphorus atoms in the vicinity of the peptide (within 1 nm of the peptide) for each force field. The enlarged images I and II show the distance between the COM of phosphates (black line) and 5 amino acids at each terminus.

biomembrane interface were studied here. First, the positioning of the model peptide WALP23 in a DOPC bilayer was studied and compared to experimental data.[71] In the second step, the positioning of the more complex SNARE peptide synaptobrevinII (short sybII) with a polyvaline transmembrane stretch was studied (sequence: 86-YWWKNLKMMVVVVVVVVV-VVVVVVVYFST-116). The tilt of both peptides and the local membrane thickness around the synaptobrevin mutant were compared for the different force field combinations (see Table 2). Moreover, for the synaptobrevin peptide the distance between the center of mass (COM) of the lipid bilayer and the center of mass of every amino acid is shown in Figure 6.

The tilt angles of the WALP23 peptide were similar for the different studied different force fields (only CHARMM36 resulted in a slightly smaller tilt angle by ≈4°) and show a good agreement to experiment.[71] A direct comparison of simulation and experimental data by comparison of quadrupolar splittings of alanine side chains did not yield significant differences between the force fields (see Supporting Information, Figure S3) on the studied time scale of 500 ns. Deviations were in the similar range as reported earlier by Monticelli et al.[73] for WALP23 using microsecond coarse-grained simulations.

All sybII peptides adopted a similar orientation in the bilayer with Lys[91] determining the tilt direction (data not shown) in agreement with a previous study.[52] However, the degree of sybII peptide tilting differed drastically among the force fields; the average peptide tilt amounts between 18.9° for GROMOS54a7 and 30.2° in Amber14sb/Lipid14 (see Table 2 for all values and standard deviations). Thereby, the peptide tilt depends on both the membrane thickness and the insertion depth of anchoring residues. Accordingly, the thickness of a pure POPC bilayer was determined to 3.94 nm for GROMOS54a7, the thickest membrane, followed by CHARMM36 (3.90 nm), Amber14sb/Lipid14 (3.78 nm), and Amber14sb/Slipids (3.75 nm).

The membrane in Amber14sb/Slipids displayed a significant thinning by ≈0.1 nm close to the sybII TM mutant peptide. Also, the local membrane thickness was observed to be correlated to the peptide tilt (see Supporting Information, Figure S5). The differences in peptide tilt are as well reflected by the relative positioning of the peptide anchor residues: the insertion depths of Trp[89] and Trp[90] in GROMOS54a7 differed from the other force fields, i.e. the residue Trp[89] is found outside the phosphate layer in GROMOS54a7 but underneath the phosphate layer in the other studied force fields (see Figure 6, Inset I). Probably the seemingly larger polarity of Trp in GROMOS54a7 is coupled to the observed partial unfolding of the peptide's termini in this force field (see Supporting Information for further details). In summary, the positioning and the secondary structure stability of the studied sybII TM mutant peptide were similar for CHARMM36 and the force field combinations Amber14sb/Lipid14 and Amber14sb/

DOI: 10.1021/acs.jctc.7b00001
J. Chem. Theory Comput. 2017, 13, 2310−2321

Slipids, while the corresponding observables differed significantly for the GROMOS54a7 force field.

3.3. Absorption of Wimley-White Peptides to the Membrane Interface. In a next step, the insertion depths of different peptides absorbed to the membrane interface were addressed. Here, submicrosecond simulations (500 ns) of selected Wimley-White (WW) peptides served as a probe. WW peptides are short unstructured peptides of sequence Ace-W_1-L_2-X_3-L_4-L_5-COO^- (X_3 denotes the probed amino acid) that were designed experimentally to position at the membrane-water interface[34] (see Figure 2 B). However, as the peptide backbone is not fully flexible (allowed regions in the Ramachandran plot)[74] not all side chains can point to the membrane interior simultaneously. Therefore, even a small difference in the hydrophobicity of residue X_3 may result in a different insertion depth of this residue and of its neighbors at the membrane interface. A comparison of the insertion depth distribution of the central residue (X_3) of the WW peptide is shown for three amino acids (charged Lys, polar Ser, and hydrophobic Phe) with differing physicochemical characteristics for the four studied force field combinations in Figure 7; other peptides are shown in the Supporting Information.

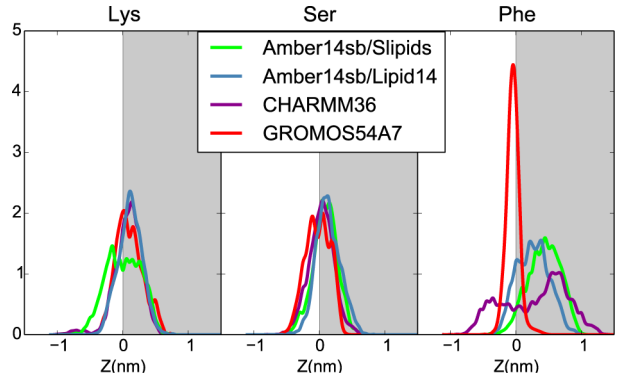

Figure 7. Insertion depth distributions (the COM of local phosphates within 1 nm corresponds to 0) of the side chain of the central residue X in three evaluated WW peptides (Lys, Ser, and Phe) using different force fields. The hydrophobic core of the bilayer is represented by the gray shadow.

With the exception of the WW peptide harboring a glutamic acid in its central position (WW_Glu) using the Amber14sb/Slipids force fields which desorbed for about 3 ns, all peptides stayed absorbed at the membrane interface during the 500 ns simulations, in agreement with their predicted position parallel to the membrane surface. The anchoring by tryptophan on the N-terminus and by the negatively charged C-terminus restrains the peptides termini to the membrane interface, thereby preventing a deep membrane burial of the central amino acids. The insertion depths of the central amino acids vary significantly depending on the force field (see e.g. Phe depth distribution as described by GROMOS54a7 or CHARMM36 in Figure 7). The expected increased insertion depth of the hydrophobic amino acid phenylalanine as compared to lysine and serine was observed for CHARMM36, but the difference was more subtle for Lipid14, Slipids, and GROMOS54a7. Counterintuitively, GROMOS54a7 showed a narrow and sharp peak for phenylalanine significantly shifted outside of the membrane as compared to the other studied force fields. Overall, the observed differences hint to significant differences in the protein−lipid interaction at the membrane interface. The following section aims to quantify these differences by analyzing the potential of the mean force (PMF) for the membrane insertion of capped amino acids.

3.4. Profiles of Uncapped Amino Acids. The potential of the mean force (PMF) as a function of the distance from the membrane center was analyzed using umbrella sampling for the uncapped amino acids Ala, Leu, Phe, Trp, Ser, Glu, Asp, and Lys for each studied force field (see Methods, results are summarized in Figure 8).

The differences between GROMOS54a7 and the other force fields are striking, e.g. the energy required to move Asp to the bilayer center (z = 0) can be up to 10 kcal/mol larger for GROMOS54a7 as compared to Amber14sb/Lipid14. Moreover, GROMOS54a7 yields the largest negative insertion energies for all amino acids as compared to the other force fields. Other more subtle differences, in particular for the position of the energy minima, that determine the preferred location of the amino acid in the bilayer, are observed as well. E.g., the minimum in the PMF for phenylalanine is located at −0.6 nm (region I), −0.9 nm (region II), −0.8 nm (region I), or −1.0 nm (region II) in GROMOS54a7, CHARMM36, Amber14sb/Slipids, and Amber14sb/Lipid14, respectively. The positively charged residue Lys, which has the ability to snorkel from the hydrophobic region to the membrane interface,[75] would be expected to display a shallow and broad potential trough within the membrane. A corresponding PMF profile was observed for CHARMM36 and Amber14sb/Slipids. Surprisingly, the GROMOS54a7 PMF profile for Lys resembles the one for the uncharged Lys (LysN). The Amber14sb/Lipid14 force field resulted in similar energy profiles for all three charged residues (Glu, Asp, and Lys).

Additionally, all force fields except for CHARMM36 displayed a significant energy minimum for the small polar residues Ser and protonated Asp (AspH) within the membrane interface region, suggesting that polar amino acids in these force fields prefer to be bound to the lipid headgroups to being fully solvated. While all force fields yielded negative insertion energy for uncapped Leu at the bilayer center, only GROMOS54a7 assigned a negative PMF to Phe in this region. Noteworthy, in all force fields Trp shows a broad minimum fully spanning over region II and partially extending into regions I and III. This broad minimum contradicts the expected preference of Trp for the membrane interface and its function in anchoring membrane proteins or peptides at a specific insertion depth (see e.g. ref 76).

3.5. Validation of Linear Membrane Absorption Free Energy for Peptides. Free energy estimates for the absorption of peptides to membranes are severely hampered by the required long sampling times, partly due to the slow equilibration of the lipid−water interface.[77]

Here, we suggest a linear interaction energy approach for estimating the membrane absorption energy of peptides ('LIMA'). I.e., the total peptide absorption energy is approximated by the sum of the absorption energies of the (isolated) residues, weighted by the respective depth distribution of the residues within the full peptide (see Methods section, eq 1). The accuracy of the LIMA approach was investigated for three representative dipeptides (Ace-W-L-NH_2, Ace-S-L-NH_2, and Ace-L-L-COO^-), by comparison of the LIMA energies to corresponding full potential of mean force (PMF) analysis for these peptides within the CHARMM36 force field.

DOI: 10.1021/acs.jctc.7b00001
J. Chem. Theory Comput. 2017, 13, 2310−2321

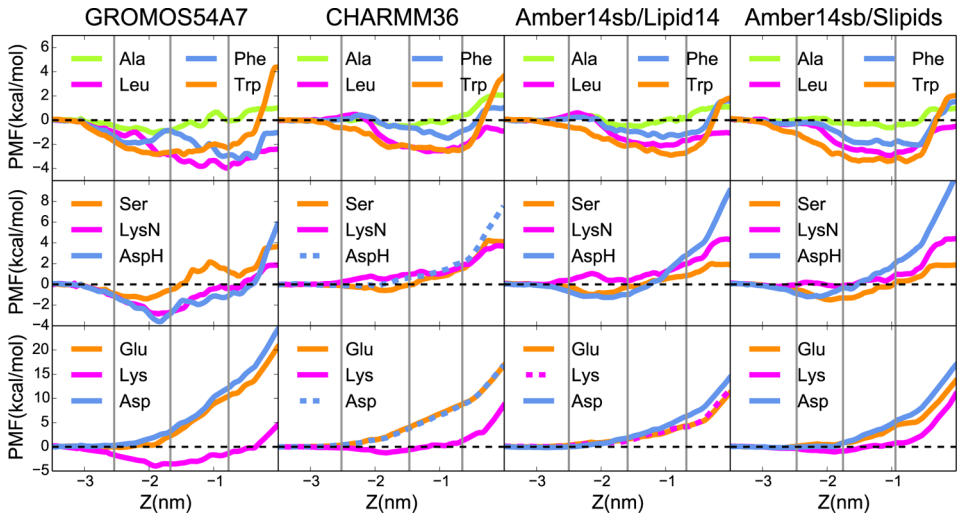

Figure 8. PMF for membrane insertion (z = 0 corresponds to the membrane center) of uncapped amino acids ordered according to their hydrophobicity. The hydrophobic Ala, Leu, Phe, and Trp amino acids are shown in the first row, the uncharged polar residues Ser, neutral Lys (LysN), and neutral Asp (AspH) are shown in the second row, and the charged residues Lys, Asp, and Glu are shown in the bottom panel. The gray lines separate the system into regions I–IV as suggested by Marrink et al.,[67] and they are calculated from the density composition of the membranes for each studied force field combination.

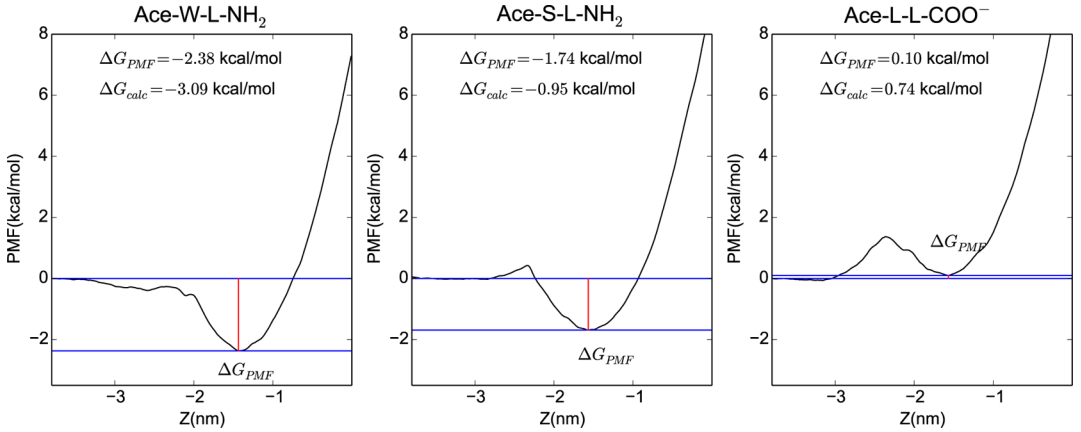

Figure 9. PMF of membrane insertion of dipeptides Ace-W-L-NH_2, Ace-S-L-NH_2, and Ace-L-L-COO^- as a function of distance from the center of mass of the lipid bilayer. The energy difference ΔG_{PMF} between the peptide in water and the absorbed peptide is given as a red line. ΔG_{calc} is the LIMA free energy estimate (see Methods).

The PMF was analyzed as a function of the distance between the COM of the membrane and the COM of the dipeptide (Figure 9). All three dipeptides exhibit an energy minimum in the membrane interface region at a distance of ≈1.6 nm from the membrane center. The presence of a significant desorption barrier in the case of the most polar dipeptide (Ace-L-L-COO^-) keeps this peptide stably absorbed to the lipid bilayer interface on the 500 ns time scale despite a vanishingly small insertion free energy. The two more hydrophobic peptides Ace-W-L-NH_2 and Ace-S-L-NH_2 both show a strong preference for the membrane interface over the water phase with absorption free energies of −1.74 kcal/mol for Ace-S-L-NH_2 and of −2.38 kcal/mol for the more hydrophobic Ace-W-L-NH_2 peptide.

The free energy difference between the peptide in bulk water and at the membrane interface (ΔG_{PMF}) was compared with the insertion energy calculated using the LIMA approach (ΔG_{calc}). The LIMA energies reproduced the same order of the peptides, with deviations between the full PMF energies and the LIMA energies below 0.8 kcal/mol, however at a significantly reduced computational cost. The linear interaction energy approach was subsequently applied to full Wimley-White peptides.

3.6. Insertion Energy of Wimley-White Peptides. The total insertion energies of different WW peptides were approximated by adding up the energetic contributions of each residue of the WW peptides, weighted by its membrane insertion depth distribution in simulations of the full peptides (see Methods section). Figure 10 shows the absolute insertion energies for eight different WW peptides in the four studied force fields compared to the experimental transfer energies between water and the bilayer interface (Wimley and White[34]). Both the correlation coefficient (R), measuring the linear correlation between experimental and calculated values, as well as the P-value, i.e. the probability to obtain the same calculated values by random sampling, are provided. CHARMM36, Amber14sb/Lipid14, and Amber14sb/Slipids force fields displayed a high linear correlation to experiment (R > 0.8), CHARMM36 being the one with the highest R-value and the smallest P-value. Although the Amber14sb/Slipids force field shows a high correlation to experiments, the insertion energies

DOI: 10.1021/acs.jctc.7b00001
J. Chem. Theory Comput. 2017, 13, 2310−2321

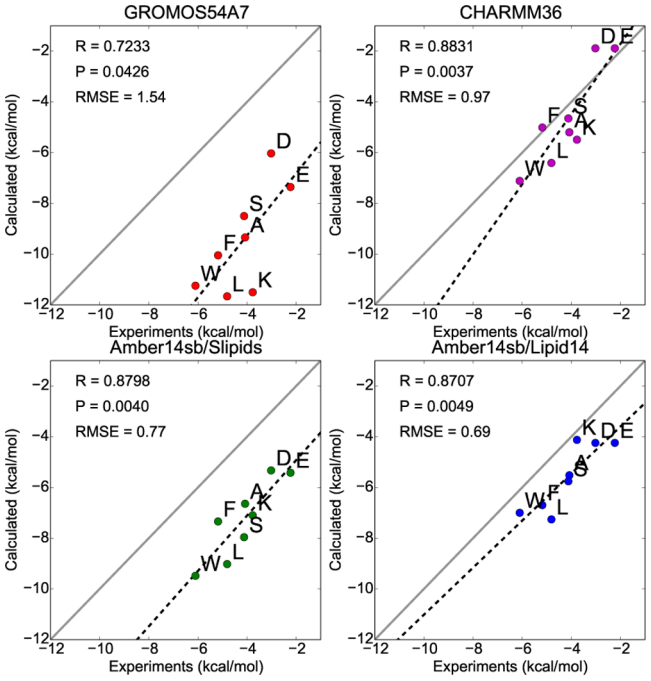

Figure 10. Comparison of absolute energies for the transfer of WW peptides between water and the bilayer interface for the studied force fields. The full line shows the ideal correlation to experimental values,[34] while the dashed line represents the actual correlation between the calculated and the experimental values in each case. The error is displayed as the root-mean-square error (RMSE).

were overall shifted to lower values (by 2.74 kcal/mol on average). GROMOS54a7 showed the worst correlation coefficient ($R < 0.75$). Similar to Amber14sb/Slipids, the WW peptide membrane absorption was overall too favorable in GROMOS54a7.

Additionally, insertion energies relative to the alanine WW peptide were calculated by subtracting the absolute membrane insertion energy of the alanine WW peptide from the WW peptide of interest, similar to the construction of the Wimley-White interface scale.[34] The force fields can be ranked by their ability to reproduce the experimental values in the following order: CHARMM36, Amber14sb/Slipids, Amber14sb/Lipid14, and GROMOS54a7. All studied force fields, with the exception of GROMOS54a7, yielded an improved correlation to experiment as compared to a previous free energy analysis for side chain analogs using a combination of the OPLS-AA[78] force field for proteins and the Berger[79] force field for DOPC lipids (see Figure 11).[80]

4. DISCUSSION AND CONCLUSIONS

Different atomistic force fields frequently used in biomembrane MD simulations were assessed focusing in particular on the description of protein−lipid interactions. Our results show that albeit the conservation of the secondary structure of transmembrane proteins is essential, it is not a sufficient criterion for the evaluation of protein−lipid interactions in atomistic force fields. The secondary structure of OmpX and AQP0 was equally well conserved for Amber14sb/Lipid14 and Amber14sb/Slipids force field combinations and the CHARMM36 force field, as well as the orientation and insertion depth of an α-helical transmembrane peptide in a model phospholipid bilayer. GROMOS54a7 showed significant differences in both structure conservation of transmembrane proteins and positioning of transmembrane peptides as compared with the other three force fields. Thus, conclusions drawn from MD studies on the interactions both of transmembrane[52] and membrane adsorbed[81] proteins with lipid membranes may significantly depend on the chosen force field. Additionally, the amino acid membrane insertion depth and the transfer free energy to the membrane interface differed significantly among the force fields. However, validation and rating of the different force fields ultimately depends on a comparison of observables to experiment. The widely applied Wimley-White scale constitutes such an experimentally well-tested observable for peptide-membrane interactions. Atomistic scale simulations of full peptides addressing their binding free energy to membranes are, however, still computationally prohibitively expensive.

In the here developed methodology the membrane insertion energies of WW peptides are approximated by the sum of the individual contributions of the single (uncapped) amino acids weighted by their insertion depth distributions as obtained from unrestrained (equilibrium) simulations of WW peptides at the membrane interface. By applying this methodology, the insertion energies of eight WW peptides in four force field combinations, namely GROMOS54a7, CHARMM36, Amber14sb/Lipid14, and Amber14sb/Slipids, were estimated and compared to experiment.

Overall, the observed peptide-membrane configurations are in agreement with the experimentally anticipated orientation of Wimley-White peptides parallel to the membrane interface, firmly anchored by the tryptophan residue on the N-terminus and by a negatively charged C-terminus. Differently, the best

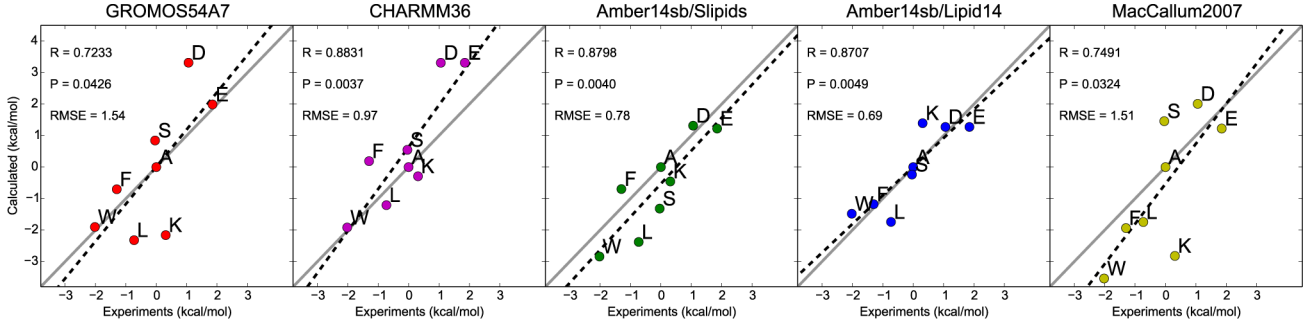

Figure 11. Comparison of calculated side chain insertion energies to a POPC bilayer interface to experiment. The diagonal line shows the ideal correlation to experimental values, while the dashed line represents the actual correlation between calculated and experimental values. The MacCallum data[80] obtained using the OPLS-AA force field for side chain analogs and the Berger force field[79] for DOPC lipids is included for comparison. The root-mean-square error (RMSE) is shown.

DOI: 10.1021/acs.jctc.7b00001
J. Chem. Theory Comput. 2017, 13, 2310−2321

overall agreement to the Wimley-White insertion energy scale was achieved by the CHARMM36 force field, closely followed by Amber14sb/Lipid14 combination of force fields. Although a comparable performance was obtained for the relative side chain insertion energies applying the Amber14sb/Slipids force field combination, the absolute binding energies were significantly overestimated. Accordingly, an overabsorption of peptides on lipid membranes is to be expected. The worst correlation to experiment was obtained for the GROMOS54a7 force field ($R \approx 0.72$). These differences in the energetics are partly coupled to structural differences.

In addition to the overall differences in correlation to experiments, the detailed comparison of individual WW-peptide insertion energies shows significant differences. E.g. Amber14sb/Lipid14 inverts the order of the charged amino acids Lys, Glu, and Asp relative to experiment. Exchange of the lipid force field (Amber14sb/Slipids) leads to a drastic decrease of the Lys interface energy by 2.9 kcal/mol, thereby improving the agreement to experiments for the charged amino acids. Additionally, only CHARMM36 and the Amber14sb/Slipids combination predict the most favorable insertion energy for the Trp WW-peptide. Obviously, the different strategies in the parametrization of lipid force fields[26,31] for Amber (Slipids and Lipid14) severely affect the relative strengths of protein−lipid interactions for the different amino acids. Our results strongly discourage the mixing of lipid and protein force field parameters without detailed testing of their compatibility.

Interestingly, all investigated force fields overestimated the interfacial binding free energy of leucine. Nevertheless, given that all lipid force fields were parametrized focusing on lipid interactions and lipid membrane thermodynamics only, the here observed agreement of peptide-lipid energies to experiment is surprisingly good. The here presented results and methodology can serve as a basis for further fine-tuning of mixed force fields in the study of protein−lipid interactions.

■ ASSOCIATED CONTENT

Supporting Information

The Supporting Information is available free of charge on the ACS Publications website at DOI: 10.1021/acs.jctc.7b00001.

Figures S1−S24, Table S1, and text (PDF)

■ AUTHOR INFORMATION

Corresponding Author

*E-mail: rainer.boeckmann@fau.de.

ORCID

Rainer A. Böckmann: 0000-0002-9325-5162

Author Contributions

A.S.-P. and K.P. contributed equally to this work.

Notes

The authors declare no competing financial interest.

■ ACKNOWLEDGMENTS

A.S.-P. acknowledges financial support by the Colombian institution Colciencias (scholarship 529/2011). This work was supported by the German Science Foundation (DFG) within the Research Training Group 1962, *Dynamic Interactions at Biological Membranes − From Single Molecules to Tissue* (A.S.-P., K.P, and R.A.B.) and the SFB1027, *Physical Modeling of Non-Equilibrium Processes in Biological Systems* (project C6). Computer time was provided by the Computing Center of the University of Erlangen-Nürnberg (RRZE).

■ REFERENCES

(1) Wallin, E.; Heijne, G. V. Genome-wide Analysis of Integral Membrane Proteins from Eubacterial, Archaean, and Eukaryotic Organisms. *Protein Sci.* **1998**, *7*, 1029−1038.

(2) Taylor, J.; Whiteford, N. E.; Bradley, G.; Watson, G. W. Validation of All-Atom Phosphatidylcholine Lipid Force Fields in the Tensionless NPT Ensemble. *Biochim. Biophys. Acta, Biomembr.* **2009**, *1788*, 638−649.

(3) Sandoval, A.; Eichler, S.; Madathil, S.; Reeves, P. J.; Fahmy, K.; Böckmann, R. A. The Molecular Switching Mechanism at the Conserved D(E)RY Motif in Class-A GPCRs. *Biophys. J.* **2016**, *111*, 79−89.

(4) Dawaliby, R.; Trubbia, C.; Delporte, C.; Masureel, M.; Van Antwerpen, P.; Kobilka, B. K.; Govaerts, C. Allosteric Regulation of G-Protein-Coupled Receptor Activity by Phospholipids. *Nat. Chem. Biol.* **2016**, *12*, 35−39.

(5) Chawla, U.; Jiang, Y.; Zheng, W.; Kuang, L.; Perera, S. M.; Pitman, M. C.; Brown, M. F.; Liang, H. A Usual G-Protein-Coupled Receptor in Unusual Membranes. *Angew. Chem., Int. Ed.* **2016**, *55*, 588−592.

(6) Nguyen, D. H.; Taub, D. CXCR4 Function Requires Membrane Cholesterol: Implications for HIV Infection. *J. Immunol.* **2002**, *168*, 4121−4126.

(7) Pluhackova, K.; Gahbauer, S.; Kranz, F.; Wassenaar, T. A.; Böckmann, R. A. Dynamic Cholesterol-Conditioned Dimerization of the G-protein Coupled Chemokine Receptor Type 4. *PLoS Comput. Biol.* **2016**, *12*, e1005169.

(8) Neale, C.; Herce, H. D.; Pomès, R.; García, A. E. Can Specific Protein-Lipid Interactions Stabilize an Active State of the Beta 2 Adrenergic Receptor? *Biophys. J.* **2015**, *109*, 1652−1662.

(9) McCammon, J. A.; Gelin, B. R.; Karplus, M. Dynamics of Folded Proteins. *Nature* **1977**, *267*, 585−590.

(10) Warshel, A.; Levitt, M. Theoretical Studies of Enzymic Reactions: Dielectric, Electrostatic and Steric Stabilization of the Carbonium Ion in the Reaction of Lysozyme. *J. Mol. Biol.* **1976**, *103*, 227−249.

(11) Weiner, P. K.; Kollman, P. A. AMBER: Assisted Model Building with Energy Refinement. A General Program for Modeling Molecules and their Interactions. *J. Comput. Chem.* **1981**, *2*, 287−303.

(12) Brooks, B. R.; Bruccoleri, R. E.; Olafson, B. D.; States, D. J.; Swaminathan, S.; Karplus, M. CHARMM: A Program for Macromolecular Energy, Minimization, and Dynamics Calculations. *J. Comput. Chem.* **1983**, *4*, 187−217.

(13) Van Gunsteren, W.; Berendsen, H. Groningen Molecular Simulation (GROMOS) Library Manual. *Biomos, Groningen* **1987**, *24*, 13.

(14) Cornell, W. D.; Cieplak, P.; Bayly, C. I.; Gould, I. R.; Merz, K. M.; Ferguson, D. M.; Spellmeyer, D. C.; Fox, T.; Caldwell, J. W.; Kollman, P. A. A Second Generation Force Field for the Simulation of Proteins, Nucleic Acids, and Organic Molecules. *J. Am. Chem. Soc.* **1995**, *117*, 5179−5197.

(15) Jorgensen, W. L.; Tirado-Rives, J. The OPLS [Optimized Potentials for Liquid Simulations] Potential Functions for Proteins, Energy Minimizations for Crystals of Cyclic Peptides and Crambin. *J. Am. Chem. Soc.* **1988**, *110*, 1657−1666.

(16) Schmid, N.; Eichenberger, A. P.; Choutko, A.; Riniker, S.; Winger, M.; Mark, A. E.; van Gunsteren, W. F. Definition and Testing of the GROMOS Force-Field Versions 54A7 and 54B7. *Eur. Biophys. J.* **2011**, *40*, 843−856.

(17) Lindorff-Larsen, K.; Piana, S.; Palmo, K.; Maragakis, P.; Klepeis, J. L.; Dror, R. O.; Shaw, D. E. Improved Side-Chain Torsion Potentials for the Amber ff99SB Protein Force Field. *Proteins: Struct., Funct., Bioinf.* **2010**, *78*, 1950−1958.

(18) Wickstrom, L.; Okur, A.; Simmerling, C. Evaluating the Performance of the ff99SB Force Field Based on NMR Scalar Coupling Data. *Biophys. J.* **2009**, *97*, 853−856.

(19) Maier, J. A.; Martinez, C.; Kasavajhala, K.; Wickstrom, L.; Hauser, K. E.; Simmerling, C. ff14SB: Improving the Accuracy of Protein Side Chain and Backbone Parameters from ff99SB. *J. Chem. Theory Comput.* **2015**, *11*, 3696−3713.
(20) Huang, J.; MacKerell, A. D. CHARMM36 All-Atom Additive Protein Force Field: Validation Based on Comparison to NMR Data. *J. Comput. Chem.* **2013**, *34*, 2135−2145.
(21) Lindorff-Larsen, K.; Maragakis, P.; Piana, S.; Eastwood, M. P.; Dror, R. O.; Shaw, D. E. Systematic Validation of Protein Force Fields Against Experimental Data. *PLoS One* **2012**, *7*, e32131.
(22) Rauscher, S.; Gapsys, V.; Gajda, M. J.; Zweckstetter, M.; de Groot, B. L.; Grubmüller, H. Structural Ensembles of Intrinsically Disordered Proteins Depend Strongly on Force Field: A Comparison to Experiment. *J. Chem. Theory Comput.* **2015**, *11*, 5513−5524. PMID: 26574339.
(23) Huang, J.; Rauscher, S.; Nawrocki, G.; Ran, T.; Feig, M.; de Groot, B. L.; Grubmüller, H.; MacKerell, A. D. CHARMM36m: An Improved Force Field for Folded and Intrinsically Disordered Proteins. *Nature Methods* **2017**, *14*, 71−73.
(24) Pastor, R.; MacKerell, A., Jr Development of the CHARMM Force Field for Lipids. *J. Phys. Chem. Lett.* **2011**, *2*, 1526−1532.
(25) Reif, M. M.; Winger, M.; Oostenbrink, C. Testing of the GROMOS Force-Field Parameter Set 54A8: Structural Properties of Electrolyte Solutions, Lipid Bilayers, and Proteins. *J. Chem. Theory Comput.* **2013**, *9*, 1247−1264.
(26) Dickson, C. J.; Madej, B. D.; Skjevik, Å. A.; Betz, R. M.; Teigen, K.; Gould, I. R.; Walker, R. C. Lipid14: the Amber Lipid Force Field. *J. Chem. Theory Comput.* **2014**, *10*, 865−879.
(27) Dickson, C. J.; Rosso, L.; Betz, R. M.; Walker, R. C.; Gould, I. R. GAFFlipid: A General Amber Force Field for the Accurate Molecular Dynamics Simulation of Phospholipid. *Soft Matter* **2012**, *8*, 9617−9627.
(28) Pluhackova, K.; Kirsch, S. A.; Han, J.; Sun, L.; Jiang, Z.; Unruh, T.; Böckmann, R. A. A Critical Comparison of Biomembrane Force Fields: Structure and Dynamics of Model DMPC, POPC, and POPE Bilayers. *J. Phys. Chem. B* **2016**, *120*, 3888−3903.
(29) Botan, A.; Favela-Rosales, F.; Fuchs, P. F. J.; Javanainen, M.; Kanduč, M.; Kulig, W.; Lamberg, A.; Loison, C.; Lyubartsev, A.; Miettinen, M. S.; Monticelli, L.; Määttä, J.; Ollila, O. H. S.; Retegan, M.; Róg, T.; Santuz, H.; Tynkkynen, J. Toward Atomistic Resolution Structure of Phosphatidylcholine Headgroup and Glycerol Backbone at Different Ambient Conditions. *J. Phys. Chem. B* **2015**, *119*, 15075−15088.
(30) Ollila, O. S.; Pabst, G. Atomistic Resolution Structure and Dynamics of Lipid Bilayers in Simulations and Experiments. *Biochim. Biophys. Acta, Biomembr.* **2016**, *1858*, 2512−2528.
(31) Jämbeck, J. P.; Lyubartsev, A. P. An Extension and Further Validation of an All-Atomistic Force Field for Biological Membranes. *J. Chem. Theory Comput.* **2012**, *8*, 2938−2948.
(32) Singh, G.; Tieleman, D. P. Using the Wimley-White Hydrophobicity Scale as a Direct Quantitative Test of Force Fields: The Martini Coarse-Grained Model. *J. Chem. Theory Comput.* **2011**, *7*, 2316−2324.
(33) de Jong, D. H.; Singh, G.; Bennett, W. D.; Arnarez, C.; Wassenaar, T. A.; Schäfer, L. V.; Periole, X.; Tieleman, D. P.; Marrink, S. J. Improved Parameters for the Martini Coarse-Grained Protein Force Field. *J. Chem. Theory Comput.* **2013**, *9*, 687−697.
(34) Wimley, W. C.; White, S. H. Experimentally Determined Hydrophobicity Scale for Proteins at Membrane Interfaces. *Nat. Struct. Biol.* **1996**, *3*, 842−848.
(35) Singh, G.; Tieleman, D. P. Atomistic Simulations of Wimley-White Pentapeptides: Sampling of Structure and Dynamics in Solution. *J. Chem. Theory Comput.* **2013**, *9*, 1657−1666.
(36) MacCallum, J. L.; Bennett, W. D.; Tieleman, D. P. Partitioning of Amino Acid Side Chains into Lipid Bilayers: Results from Computer Simulations and Comparison to Experiment. *J. Gen. Physiol.* **2007**, *129*, 371−377.
(37) Sun, D.; Forsman, J.; Woodward, C. E. Evaluating Force Fields for the Computational Prediction of Ionized Arginine and Lysine Side-Chains Partitioning into Lipid Bilayers and Octanol. *J. Chem. Theory Comput.* **2015**, *11*, 1775−1791.
(38) Best, R. B.; Zhu, X.; Shim, J.; Lopes, P. E. M.; Mittal, J.; Feig, M.; MacKerell, A. D. Optimization of the Additive CHARMM All-Atom Protein Force Field Targeting Improved Sampling of the Backbone ϕ, ψ and Side-Chain χ1 and χ2 Dihedral Angles. *J. Chem. Theory Comput.* **2012**, *8*, 3257−3273.
(39) Case, D.; Babin, V.; Berryman, J.; Betz, R.; Cai, Q.; Cerutti, D.; Cheatham, T., III; Darden, T.; Duke, R.; Gohlke, H.; Goetz, A.; Gusarov, S.; Homeyer, N.; Janowski, P.; Kaus, J.; Kolossváry, I.; Kovalenko, A.; Lee, T.; LeGrand, S.; Luchko, T.; Luo, R.; Madej, B.; Merz, K.; Paesani, F.; Roe, D.; Roitberg, A.; Sagui, C.; Salomon-Ferrer, R.; Seabra, G.; Simmerling, C.; Smith, W.; Swails, J.; Walker, R.; Wang, J.; Wolf, R.; Wu, X.; Kollman, P. *AMBER 14*; 2014.
(40) Jämbeck, J. P.; Lyubartsev, A. P. Derivation and Systematic Validation of a Refined All-Atom Force Field for Phosphatidylcholine Lipids. *J. Phys. Chem. B* **2012**, *116*, 3164−3179. PMID: 22352995.
(41) Hagn, F.; Etzkorn, M.; Raschle, T.; Wagner, G. Optimized Phospholipid Bilayer Nanodiscs Facilitate High-Resolution Structure Determination of Membrane Proteins. *J. Am. Chem. Soc.* **2013**, *135*, 1919−1925.
(42) Gonen, T.; Cheng, Y.; Sliz, P.; Hiroaki, Y.; Fujiyoshi, Y.; Harrison, S. C.; Walz, T. Lipid-Protein Interactions in Double-Layered Two-Dimensional AQP0 Crystals. *Nature* **2005**, *438*, 633−638.
(43) Pluhackova, K.; Wassenaar, T. A.; Böckmann, R. A. Molecular Dynamics Simulations of Membrane Proteins. *Methods Mol. Biol.* **2013**, *1033*, 85−101.
(44) de Jong, D. H.; Singh, G.; Bennett, W. F. D.; Arnarez, C.; Wassenaar, T. A.; Schäfer, L. V.; Periole, X.; Tieleman, D. P.; Marrink, S. J. Improved Parameters for the Martini Coarse-Grained Protein Force Field. *J. Chem. Theory Comput.* **2013**, *9*, 687−697.
(45) Wassenaar, T. A.; Ingolfsson, H. I.; Böckmann, R. A.; Tieleman, D. P.; Marrink, S. J. Computational Lipidomics with *insane*: A Versatile Tool for Generating Custom Membranes for Molecular Simulations. *J. Chem. Theory Comput.* **2015**, *11*, 2144−2155.
(46) Berendsen, H. J. C.; Postma, J. P. M.; van Gunsteren, W. F.; DiNola, A.; Haak, J. R. Molecular Dynamics with Coupling to an External Bath. *J. Chem. Phys.* **1984**, *81*, 3684−3690.
(47) Wassenaar, T. A.; Pluhackova, K.; Böckmann, R. A.; Marrink, S. J.; Tieleman, D. P. Going Backward: A Flexible Geometric Approach to Reverse Transformation from Coarse Grained to Atomistic Models. *J. Chem. Theory Comput.* **2014**, *10*, 676−690.
(48) Aqvist, J. Ion-Water Interaction Potentials Derived from Free Energy Perturbation Simulations. *J. Phys. Chem.* **1990**, *94*, 8021−8024.
(49) Joung, I. S.; Cheatham, T. E., III Determination of Alkali and Halide Monovalent Ion Parameters for Use in Explicitly Solvated Biomolecular Simulations. *J. Phys. Chem. B* **2008**, *112*, 9020−9041.
(50) Skjevik, A. A.; Madej, B. D.; Dickson, C. J.; Lin, C.; Teigen, K.; Walker, R. C.; Gould, I. R. Simulation of Lipid Bilayer Self-Assembly Using All-Atom Lipid Force Fields. *Phys. Chem. Chem. Phys.* **2016**, *18*, 10573−10584.
(51) Jämbeck, J. P. M.; Lyubartsev, A. P. Another Piece of the Membrane Puzzle: Extending Slipids Further. *J. Chem. Theory Comput.* **2013**, *9*, 774−784.
(52) Han, J.; Pluhackova, K.; Bruns, D.; Böckmann, R. A. Synaptobrevin Transmembrane Domain Determines the Structure and Dynamics of the SNARE Motif and the Linker Region. *Biochim. Biophys. Acta, Biomembr.* **2016**, *1858*, 855−865.
(53) Schrödinger, LLC *The PyMOL Molecular Graphics System, Version 1.3*; Schrödinger, LLC.
(54) Kirkwood, J. G. Statistical Mechanics of Fluid Mixtures. *J. Chem. Phys.* **1935**, *3*, 300−313.
(55) Torrie, G. M.; Valleau, J. P. Nonphysical Sampling Distributions in Monte Carlo Free-Energy Estimation: Umbrella Sampling. *J. Comput. Phys.* **1977**, *23*, 187−199.
(56) Abraham, M. J.; Murtola, T.; Schulz, R.; Páll, S.; Smith, J. C.; Hess, B.; Lindahl, E. GROMACS: High Performance Molecular Simulations Through Multi-level Parallelism from Laptops to Supercomputers. *SoftwareX* **2015**, *1-2*, 19−25.

DOI: 10.1021/acs.jctc.7b00001
J. Chem. Theory Comput. 2017, 13, 2310−2321

(57) Tironi, I. G.; Sperb, R.; Smith, P. E.; van Gunsteren, W. F. A Generalized Reaction Field Method for Molecular Dynamics Simulations. *J. Chem. Phys.* **1995**, *102*, 5451−5459.
(58) Darden, T.; York, D.; Pedersen, L. Particle Mesh Ewald: An N · log(N) Method for Ewald Sums in Large Systems. *J. Chem. Phys.* **1993**, *98*, 10089−10092.
(59) Parrinello, M.; Rahman, A. Polymorphic Transitions in Single Crystals: A New Molecular Dynamics Method. *J. Appl. Phys.* **1981**, *52*, 7182−7190.
(60) Páll, S.; Hess, B. A Flexible Algorithm for Calculating Pair Interactions on {SIMD} Architectures. *Comput. Phys. Commun.* **2013**, *184*, 2641−2650.
(61) Shirts, M. R.; Mobley, D. L.; Chodera, J. D.; Pande, V. S. Accurate and Efficient Corrections for Missing Dispersion Interactions in Molecular Simulations. *J. Phys. Chem. B* **2007**, *111*, 13052−13063.
(62) Nosé, S. A. Molecular Dynamics Method for Simulations in the Canonical Ensemble. *Mol. Phys.* **2002**, *100*, 191−198.
(63) Hoover, W. G. Canonical Dynamics: Equilibrium Phase-Space Distributions. *Phys. Rev. A: At., Mol., Opt. Phys.* **1985**, *31*, 1695−1697.
(64) Berendsen, H. J. C.; Postma, J. P. M.; van Gunsteren, W. F.; Hermans, J. Interaction Models for Water in Relation to Protein Hydration. *Intermolecular Forces* **1981**, *14*, 331−342.
(65) MacKerell, A. D.; Bashford, D.; Bellott; Dunbrack, R. L.; Evanseck, J. D.; Field, M. J.; Fischer, S.; Gao, J.; Guo, H.; Ha, S.; Joseph-McCarthy, D.; Kuchnir, L.; Kuczera, K.; Lau, F. T. K.; Mattos, C.; Michnick, S.; Ngo, T.; Nguyen, D. T.; Prodhom, B.; Reiher, W. E.; Roux, B.; Schlenkrich, M.; Smith, J. C.; Stote, R.; Straub, J.; Watanabe, M.; Wiórkiewicz-Kuczera, J.; Yin, D.; Karplus, M. All-Atom Empirical Potential for Molecular Modeling and Dynamics Studies of Proteins. *J. Phys. Chem. B* **1998**, *102*, 3586−3616.
(66) Sun, Y.; Kollman, P. A. Hydrophobic Solvation of Methane and Nonbond Parameters of the TIP3P Water Model. *J. Comput. Chem.* **1995**, *16*, 1164−1169.
(67) Marrink, S. J.; De Vries, A. H.; Mark, A. E. Coarse Grained Model for Semiquantitative Lipid Simulations. *J. Phys. Chem. B* **2004**, *108*, 750−760.
(68) Klauda, J. B.; Venable, R. M.; Freites, J. A.; O'Connor, J. W.; Tobias, D. J.; Mondragon-Ramirez, C.; Vorobyov, I.; MacKerell, A. D., Jr; Pastor, R. W. Update of the CHARMM All-Atom Additive Force Field for Lipids: Validation on Six Lipid Types. *J. Phys. Chem. B* **2010**, *114*, 7830−7843.
(69) Hub, J. S.; De Groot, B. L.; Van Der Spoel, D. g_wham: A Free Weighted Histogram Analysis Implementation Including Robust Error and Autocorrelation Estimates. *J. Chem. Theory Comput.* **2010**, *6*, 3713−3720.
(70) Kabsch, W.; Sander, C. Dictionary of Protein Secondary Structure: Pattern Recognition of Hydrogen-Bonded and Geometrical Features. *Biopolymers* **1983**, *22*, 2577−2637.
(71) Strandberg, E.; Esteban-Martín, S.; Ulrich, A. S.; Salgado, J. Hydrophobic Mismatch of Mobile Transmembrane Helices: Merging Theory and Experiments. *Biochim. Biophys. Acta, Biomembr.* **2012**, *1818*, 1242−1249.
(72) Kučerka, N.; Nieh, M. P.; Katsaras, J. Fluid Phase Lipid Areas and Bilayer Thicknesses of Commonly Used Phosphatidylcholines as a Function of Temperature. *Biochim. Biophys. Acta, Biomembr.* **2011**, *1808*, 2761−2771.
(73) Monticelli, L.; Tieleman, D. P.; Fuchs, P. F. J. Interpretation of ^{2}H-NMR Experiments on the Orientation of the Transmembrane Helix WALP23 by Computer Simulations. *Biophys. J.* **2010**, *99*, 1455−1464.
(74) Ramachandran, G.; Ramakrishnan, C.; Sasisekharan, V. Stereochemistry of Polypeptide Chain Configurations. *J. Mol. Biol.* **1963**, *7*, 95−99.
(75) Strandberg, E.; Killian, J. A. Snorkeling of Lysine Side Chains in Transmembrane Helices: How Easy Can It Get? *FEBS Lett.* **2003**, *544*, 69−73.
(76) Borisovska, M.; Schwarz, Y. N.; Dhara, M.; Yarzagaray, A.; Hugo, S.; Narzi, D.; Siu, S. W.; Kesavan, J.; Mohrmann, R.; Böckmann, R. A.; Bruns, D. Membrane-proximal tryptophans of synaptobrevin II stabilize priming of secretory vesicles. *J. Neurosci.* **2012**, *32*, 15983−15997.
(77) Neale, C.; Bennett, W. F. D.; Tieleman, D. P.; Pomes, R. Statistical Convergence of Equilibrium Properties in Simulations of Molecular Solutes Embedded in Lipid Bilayers. *J. Chem. Theory Comput.* **2011**, *7*, 4175−4188.
(78) Kaminski, G.; Friesner, R. A.; Tirado-Rives, J.; Jorgensen, W. L. Evaluation and Reparametrization of the OPLS-AA Force Field for Proteins via Comparison with Accurate Quantum Chemical Calculations on Peptides. *J. Phys. Chem. B* **2001**, *105*, 6474−6487.
(79) Berger, O.; Edholm, O.; Jähnig, F. Molecular Dynamics Simulations of a Fluid Bilayer of Dipalmitoylphosphatidylcholine at Full Hydration, Constant Pressure, and Constant Temperature. *Biophys. J.* **1997**, *72*, 2002−2013.
(80) MacCallum, J. L.; Bennett, W. D.; Tieleman, D. P. Distribution of Amino Acids in a Lipid Bilayer from Computer Simulations. *Biophys. J.* **2008**, *94*, 3393−3404.
(81) Rabe, M.; Aisenbrey, C.; Pluhackova, K.; de Wert, V.; Boyle, A. L.; Bruggeman, D. F.; Kirsch, S. A.; Böckmann, R. A.; Kros, A.; Raap, J.; Bechinger, B. A Coiled-Coil Peptide Shaping Lipid Bilayers upon Fusion. *Biophys. J.* **2016**, *111*, 2162−2175.

DOI: 10.1021/acs.jctc.7b00001
J. Chem. Theory Comput. 2017, 13, 2310−2321